Xie et al. *EPJ Quantum Technology* (2026) 13:11
https://doi.org/10.1140/epjqt/s40507-025-00458-8

EPJ.org

EPJ Quantum Technology

RESEARCH Open Access

Enhancement of optomagnonic coupling and microwave-optical conversion via magnetic anisotropy

Hong Xie[1*], Le-Wei He[1], Xiang Lin[1] and Xiu-Min Lin[2,3,4*]

*Correspondence: xh@fjxu.edu.cn; xmlin@fjnu.edu.cn
[1]Department of Mathematics and Physics, Fujian Jiangxia University, Fuzhou, 350108, China
[2]Fujian Provincial Key Laboratory of Quantum Manipulation and New Energy Materials, College of Physics and Energy, Fujian Normal University, Fuzhou, 350117, China
Full list of author information is available at the end of the article

Abstract

Efficient microwave-optical frequency conversion is critical for building long-distance quantum networks. Magnons in ferromagnets offer a promising mediator for this conversion, owing to their ability to couple to both microwave and optical fields. However, the magnon-mediated microwave-optical conversion efficiency is severely limited by the inherently weak optomagnonic coupling. Here, we propose a scheme to enhance the optomagnonic coupling by utilizing the intrinsic magnetic anisotropy in a yttrium iron garnet (YIG) thin film. The presence of magnetic anisotropy establishes a squeezed vacuum for the magnonic ground state, which enhances the effective optomagnonic coupling strength by a factor of $\cosh(r)$, where r is the squeezing parameter. This results in a significant boost of the corresponding cooperativities and, consequently, the microwave-to-optical conversion efficiency by several orders of magnitude for large squeezing. Our approach harnesses magnon squeezing as an intrinsic resource to strengthen optomagnonic interactions, creating opportunities for high-efficiency microwave-optical conversion.

Keywords: Microwave-optical frequency conversion; Squeezed magnons; Enhancement

1 Introduction

The development of a microwave-optical frequency converter is crucial for quantum information processing and hybrid quantum networks [1–3]. Such a device is able to link superconducting qubits, which operate at microwave frequencies, to optical photons, which are the ideal carriers for transmitting quantum information over long distances [4]. A variety of platforms have been developed to realize coherent microwave-optical frequency conversion, such as electro-optomechanics [5–8], piezo-optomechanics [9–13], electro-optic interaction [14–19], Rydberg atoms [20–25], and erbium ions [26].

Recently, the magnon-mediated microwave-optical conversion has attracted great attention [27–33]. Magnons, the collective excitation of spins in ordered magnets, have large frequency tunability and low dissipation rate [34]. Magnons in the ferromagnetic crystal yttrium iron garnet (YIG) have been shown the ability to couple to various systems, in-

Springer

cluding microwave [35–38] and optical fields [28–30], acoustic waves [39], and superconducting qubits [40–42]. This makes the magnons an attractive candidate for constructing a magnon-based hybrid system [43–45]. Their frequency tunability via external magnetic fields makes them particularly suitable for enabling broadband microwave-optical conversion [2].

To obtain efficient magnon-mediated microwave-optical conversion, the strong coupling of magnons to both the microwave and optical photons is required. While strong coupling [35–37] and even ultrastrong coupling [38, 46] between magnons and microwave photons have been demonstrated, the optomagnonic interaction between magnons and optical photons is inherently very weak due to the small mode volume overlap [44, 45]. There have been many theoretical and experimental efforts made to reduce the mode volume and enhance mode overlap between the optical field and the magnon mode [32, 33, 47–51]. However, even with strong optical driving enhancement, the achievable optomagnonic coupling in experiments is insufficient to obtain efficient microwave-optical conversion; the current highest magnon-mediated microwave-optical conversion efficiency is about $\sim 10^{-8}$ [32, 33]. A recent approach uses both magnetic and mechanical excitations to mediate between microwave and optical photons [52]. By leveraging strong magnetoelastic and optomechanical effects, this method overcomes the limitation of weak optomagnonic coupling but comes with increased setup complexity.

Here, we propose a scheme that utilizes the intrinsic magnetic anisotropy of a YIG thin film to enhance the optomagnonic coupling. The YIG thin film manifests a strong shape anisotropy, which leads to the magnonic ground state being a squeezed vacuum state. The effective optomagnonic coupling strength and the corresponding cooperativity can be enhanced by amplification of spin fluctuations in the squeezed magnon mode. Under the triple-resonance condition, the enhanced coupling can boost the microwave-optical conversion efficiency by several orders of magnitude. Different from the method that uses time-dependent parametric driving to squeeze light and enhance the light-matter interaction [53–63], the magnon mode is intrinsically squeezed in the anisotropic ferromagnet, thus avoiding the need for external driving and associated fast-oscillating processes. Our scheme offers a stable and experimentally feasible way to enhance the optomagnonic coupling and hence the magnon-mediated microwave-optical conversion efficiency.

2 Model

The system comprises a YIG thin film simultaneously coupled to both a microwave cavity and an optical cavity. Such a configuration has been demonstrated experimentally in a YIG waveguide-based cavity [32] and Fabry-Pérot optical cavity [33]. The Hamiltonian of the system is given by

$$H_{\mathrm{sys}} = H_{\mathrm{m}} + H_{\mathrm{om}} + H_{\mathrm{em}}, \tag{1}$$

where H_{m} is the ferromagnetic Hamiltonian, H_{om} describes the optomagnonic interaction between the magnetization and the optical cavity field, and H_{em} represents the magnetic-dipole interaction between the magnetization and the microwave cavity mode.

A static magnetic field $\mathbf{B} = B_0\hat{\mathbf{z}}$ is applied to the YIG thin film along the z-direction. The ferromagnetic Hamiltonian is given as [34]

$$H_{\mathrm{m}} = -2J\sum_{\langle i,j\rangle}\mathbf{S}_i\cdot\mathbf{S}_j - g_Z\mu_B\sum_i\mathbf{B}\cdot\mathbf{S}_i \tag{2}$$

$$+\sum_i (K_x S_{ix}^2 + K_y S_{iy}^2 + K_z S_{iz}^2),$$

where $\mathbf{S}_i$ is the spin operator on the ith site, $J > 0$ represents the exchange interaction strength between the nearest-neighbor spin $\langle i,j\rangle$. The second term denotes the Zeeman energy, with g_Z being the Landé factor and μ_B the Bohr magneton. The thin film of the ferromagnet manifests a strong shape anisotropy, which arises from the dipole interaction between the demagnetization field and the magnetization [64–67]. In the last term in Eq. (2), a general form of the magnetic anisotropy with the parameters K_x, K_y, and K_z is adopted to capture this shape anisotropy, as well as possible magnetocrystalline anisotropy [34].

By applying the Holstein-Primakoff transformation [68] $S_i^+ \approx \sqrt{2S} m_i$, $S_i^- \approx \sqrt{2S} m_i^\dagger$, and $S_{iz} \approx S - m_i^\dagger m_i$, the spin operator can be expressed in terms of the bosonic annihilation (creation) operator m_i ($m_i^\dagger$), where S is the total spin. The bosonic operators defined on each site are related to the spin-wave operators $m_{\mathbf{k}}$ and $m_{\mathbf{k}}^\dagger$ via the Fourier transforms $m_i = N^{-1/2} \sum_{\mathbf{k}} m_{\mathbf{k}} e^{i\mathbf{k}\cdot\mathbf{r}_i}$, where $m_{\mathbf{k}}$ ($m_{\mathbf{k}}^\dagger$) represents the magnon annihilation (creation) operator with the wavevector $\mathbf{k}$, and N is the total number of spins in the ferromagnet. After omitting the constant term and high-order interaction terms, the ferromagnetic Hamiltonian becomes ($\hbar = 1$)

$$H_{\mathrm{m}} = \sum_{\mathbf{k}} \left[\omega(\mathbf{k}) m_{\mathbf{k}}^\dagger m_{\mathbf{k}} + \lambda (m_{\mathbf{k}}^\dagger m_{-\mathbf{k}}^\dagger + m_{\mathbf{k}} m_{-\mathbf{k}}) \right], \tag{3}$$

with the dispersion relation $\omega(\mathbf{k}) = 4JS\mathrm{k}^2 a^2 + g_Z \mu_B B_0 + (K_x + K_y - 2K_z)S$ and the anisotropic strength $\lambda = (K_x - K_y)S/2$. Here, $\mathrm{k} = |\mathbf{k}|$ is the momentum and a is the lattice parameter. The detailed derivation of Eq. (3) is present in the Appendix. In the derivation of the ferromagnetic Hamiltonian, we retain only the terms that are second order in the magnon operators. The Kerr nonlinearity, which arises from higher-order contributions, is omitted because its characteristic energy scale remains well below that of the dominant quadratic terms. This treatment is consistent with the focus on the leading-order effects of anisotropy [64–67, 69–72].

The uniform $\mathbf{k} = 0$ magnon mode is the most readily excited mode in ferromagnetic resonance experiments, and it typically dominates the coupling to cavity fields due to its spatial overlap with uniform microwave and optical modes. In contrast, efficiently coupling non-uniform magnon modes requires cavity fields with matching spatial profiles [43], thereby increasing the experimental difficulty. Therefore, we restrict our analysis to the uniform mode for simplicity. The Hamiltonian for the uniform magnon mode is expressed as

$$H_{\mathrm{m}} = \omega_m m^\dagger m + \lambda (m^{\dagger 2} + m^2), \tag{4}$$

where $m_{\mathbf{k}=\mathbf{0}}$ is abbreviated as m, and $\omega_m = g_Z \mu_B B_0 + (K_x + K_y - 2K_z)S$ is the ferromagnetic resonance frequency corresponding to the $\mathbf{k} = 0$ mode. Note that the anisotropy term introduces a squeezing property for magnons.

We now consider the coupling of magnons to optical and microwave cavity modes, a topic that has been extensively studied both theoretically and experimentally [44, 45].

The optomagnonic interaction between magnons and optical modes effectively constitutes a three-wave mixing process [73]. Under the rotating-wave approximation, the optomagnonic Hamiltonian, including the free cavity terms, is described by

$$H_{\rm om} = \omega_1 a_1^\dagger a_1 + \omega_2 a_2^\dagger a_2 + g_{\rm om}(a_1 a_2^\dagger m + a_1^\dagger a_2 m^\dagger), \tag{5}$$

where a_i ($i = 1, 2$) are the annihilation operators of the optical cavity modes with frequencies ω_i, $g_{\rm om}$ is the single-photon optomagnonic coupling strength. In typical YIG sphere-based optomagnonic systems, the single-photon magneto-optical coupling is very weak, e.g., $g_{\rm om}/2\pi \leq 1$ Hz [28–30], which limits the efficient microwave-optical conversion. Recently, the coupling has been improved to $g_{\rm om}/2\pi \approx 17$ Hz by confining the optical mode and magnon mode in a small mode volume with large mode overlap in the YIG thin film [32]. Despite this improvement, the coupling strength remains very limited for achieving high-efficiency microwave-optical conversion.

In contrast to the weak optomagnonic interaction, strong and even ultrastrong magnetic-dipole coupling between magnons and microwave cavity modes has been demonstrated [35–38, 46]. For a linearly-polarized microwave cavity field, the magnetic-dipole Hamiltonian under the rotating-wave approximation reads

$$H_{\rm em} = \omega_c c^\dagger c + g_{\rm em}(c^\dagger m + c m^\dagger), \tag{6}$$

where c is the annihilation operator of the microwave cavity mode and $g_{\rm em}$ denotes the magnetic-dipole coupling strength.

3 Enhancement of the optomagnonic coupling

Consider that one of the optical modes is strongly driven by an external field $H_{\rm d} = \Omega(a_2 e^{i\omega_L t} + a_2^\dagger e^{-i\omega_L t})$ with amplitude Ω and frequency ω_L. The strong coherence driving field can be treated classically, and the operator a_2 in the interaction Hamiltonian could be replaced with the coherent amplitude α_2. The amplitude can be obtained as $\alpha_2 = \Omega/(i\kappa_{\rm a2}/2 - \Delta_2)$ using the standard linearized process [74], where $\kappa_{\rm a2}$ is decay rates for optical mode a_2 and $\Delta_2 = \omega_2 - \omega_L$ is the driving detuning. Then the total Hamiltonian in the rotating frame of ω_L can be written as

$$H_{\rm tot} = \Delta_1 a_1^\dagger a_1 + G_{\rm om}(a_1 m^\dagger + a_1^\dagger m) + H_{\rm m} + H_{\rm em}, \tag{7}$$

where $\Delta_1 = \omega_1 - \omega_L$ and we have assume the optical mode a_2 is resonantly driven $\Delta_2 = 0$. The magneto-optical coupling $G_{\rm om} = g_{\rm om}|\alpha_2|$ is enhanced by the driving field. For a driving field with photon number $\langle n_2 \rangle = |\alpha_2|^2 = 1.77 \times 10^6$, the driving-enhanced magneto-optical coupling strength is $G_{\rm om}/2\pi = 22.59$ kHz [32]. However, this coupling strength is still insufficient to obtain a high microwave-to-optical conversion efficiency; the internal conversion efficiency is $\sim 10^{-7}$ based on this enhanced coupling in waveguide cavity optomagnonics [32].

We now show that the coupling can be further enhanced in the presence of the magnetic anisotropy. By introducing the Bogoliubov transformation

$$\beta = \cosh(r) m + \sinh(r) m^\dagger = S(r) m S^\dagger(r) \tag{8}$$

with the squeezing parameter

$$r = \frac{1}{4}\ln\left(\frac{\omega_m + 2\lambda}{\omega_m - 2\lambda}\right) \tag{9}$$

and the squeezing operator $S(r) = e^{(m^2 - m^{\dagger 2})r/2}$, the magnetic Hamiltonian $H_{\rm m} = \omega_m m^\dagger m + \lambda(m^{\dagger 2} + m^2)$ is diagonalized to

$$H_m = \omega_\beta \beta^\dagger \beta, \tag{10}$$

where the frequency of the squeezed magnon mode is

$$\omega_\beta = \sqrt{\omega_m^2 - 4\lambda^2}. \tag{11}$$

The ground state of the anisotropic ferromagnet is a squeezed state $|G\rangle = S(r)|0\rangle$, with $|0\rangle$ being the vacuum state of mode m. This squeezing arises from the interplay between energy minimization and the Heisenberg uncertainty principle [65]. As a result, the squeezed state is stabilized against decay due to the system's tendency to minimize the ground-state energy.

For the spin components $S_x = \sum_i S_{ix} = \sqrt{2NS}(m + m^\dagger)/2$ and $S_y = \sum_i S_{iy} = \sqrt{2NS}(m - m^\dagger)/2i$, the quantum fluctuations in the anisotropic ferromagnet ground state are given by

$$\Delta S_x = \sqrt{\frac{NS}{2}} e^{-r}, \tag{12a}$$

$$\Delta S_y = \sqrt{\frac{NS}{2}} e^{r}. \tag{12b}$$

The fluctuation of component S_x is squeezed, accompanied by the amplification of the fluctuation of S_y. The Wigner function of the ground state of the magnetic Hamiltonian H_m is plotted in Fig. 1(a). As compared to the isotropy case ($\lambda = 0$) in the left panel, the magnetic anisotropy introduces a squeezed fluctuation in S_x and an amplified fluctuation in S_y.

In terms of the squeezed magnon mode β, the total Hamiltonian $H_{\rm tot}$ under the rotating-wave approximation can be effectively written as

$$H_{\rm eff} = \Delta_1 a_1^\dagger a_1 + \tilde{G}_{\rm om}(a_1\beta^\dagger + a_1^\dagger\beta) + \omega_\beta\beta^\dagger\beta + \omega_c c^\dagger c + \tilde{g}_{\rm em}(c\beta^\dagger + c^\dagger\beta), \tag{13}$$

where $\tilde{G}_{\rm om} = G_{\rm om}\cosh(r)$ and $\tilde{g}_{\rm em} = g_{\rm em}\cosh(r)$. Both the effective magnetic-optical coupling $\tilde{G}_{\rm om}$ and magnetic-microwave coupling $\tilde{g}_{\rm em}$ are enhanced by a factor $\cosh(r)$, as illustrated in Fig. 1(b). This enhancement originates from the amplification of quantum fluctuations in the squeezed magnon mode. We note that while similar coupling enhancement via squeezing has been studied using time-dependent parametric driving [53–63], the intrinsic squeezing in an anisotropic ferromagnet avoids the need for external driving and associated fast-oscillating processes.

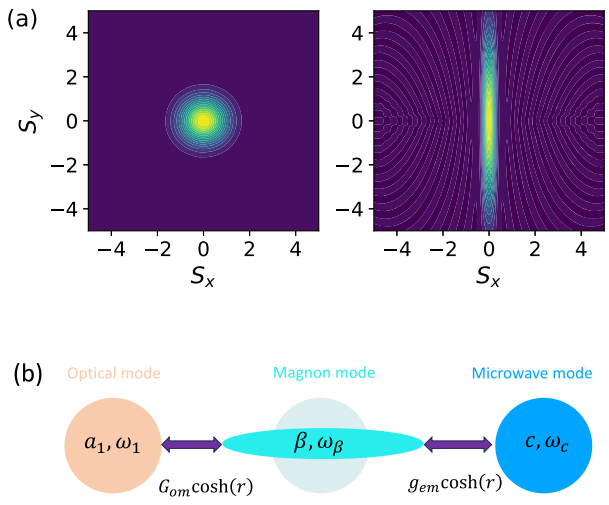

Figure 1 (Color online) (a) Wigner function of the magnetic ground state. The left panel shows the result in the absence of the magnetic anisotropy ($\lambda = 0$), and the right panel shows the squeezed fluctuation in the presence of the magnetic anisotropy ($\lambda = 0.495\omega_m$). (b) The amplified spin fluctuations enhance both the magneto-optical coupling and the magnetic-microwave coupling by a factor cosh(r)

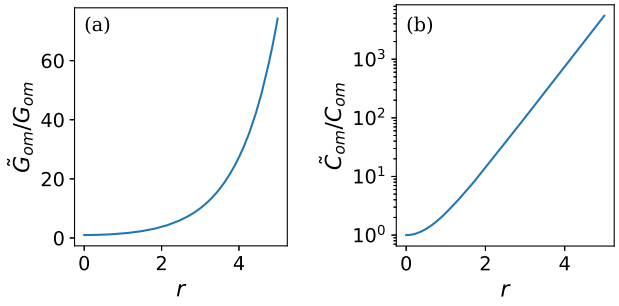

Figure 2 (Color online) (a) Coupling enhancement $\tilde{G}_{\rm om}/G_{\rm om}$ and (b) cooperativity enhancement $\tilde{C}_{\rm om}/C_{\rm om}$ as a function of the squeezing parameter r

For a squeezing parameter $r \geq 1$, the effective optomagnonic coupling scales as $\tilde{G}_{\rm om} \approx G_{\rm om}e^r/2$, exhibiting a enhancement proportional to the measurable squeezing factor e^r. In the study of microwave-optics frequency conversion, the cooperativity $C_{\rm om} = 4G_{\rm om}^2/\kappa_a\gamma$ is an important parameter to quantify the conversion efficiency, where $\kappa_{\rm a}$ and γ are the total dissipation rates of optical mode and magnon mode, respectively. In the presence of the magnon squeezing, the cooperativity $\tilde{C}_{\rm om} = 4\tilde{G}_{\rm om}^2/\kappa_a\gamma = C_{\rm om}e^{2r}/4$ is also enhanced with the factor proportional to e^{2r}. As illustrated in Fig. 2, both the coupling enhancement ratio $\tilde{G}_{\rm om}/G_{\rm om}$ and cooperativity enhancement ratio $\tilde{C}_{\rm om}/C_{\rm om}$ increase significantly with r, with the latter being enhanced by several orders of magnitude for strong squeezing. With the enhancement of coupling strength and cooperativity, the magnon-based Brillouin light scattering rate will also be improved [45]. The discussion of coupling and cooperativity enhancement is also valid for the magnon–microwave interaction. The enhanced magnetic-microwave coupling is given by $\tilde{g}_{\rm em} \approx g_{\rm em}e^r/2$, and the corresponding cooperativity becomes $\tilde{C}_{\rm em} = C_{\rm em}e^{2r}/4$, where $C_{\rm em} = 4g_{\rm em}^2/\kappa_c\gamma$ is the unsqueezed cooperativity for the magnon–microwave subsystem, and κ_c is the decay rate of the microwave

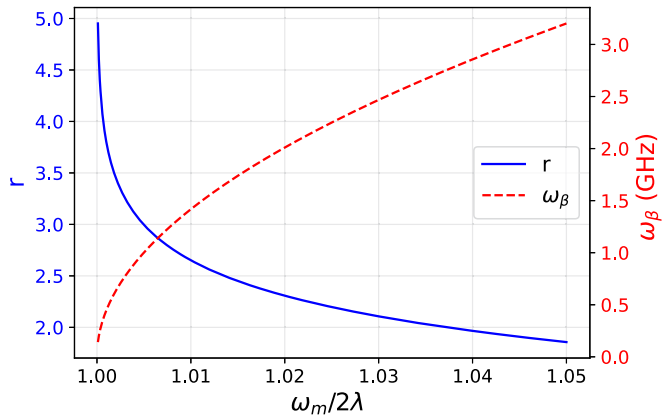

Figure 3 The squeezing parameter r and frequency of squeezed mode ω_β as a function of $\omega_m/2\lambda$, the anisotropy strength is chosen as $\lambda = 5$ GHz

cavity. While the enhanced fluctuations in the squeezed mode may also amplify higher-order nonlinear effects [75–77], our analysis focuses on the exponential enhancement of the linear optomagnonic coupling and cooperativity, which constitutes the main scope of this work.

Note that the high squeezing appears accompanied by the reduction of the frequency of the squeezed mode. There is a trade-off between the degree of squeezing and frequency. From Eqs. (9) and (11), we obtain that r sharply increases when ω_m approaches 2λ from above, but the frequency ω_β approaches zero at the same time. For a too low frequency, thermal fluctuation will destroy the coherent interaction, and it is difficult to design the cavity for optomagnonic and magnon–microwave interactions. Fortunately, with a large anisotropy strength, it is feasible to achieve high squeezing while maintaining the frequency in the GHz range. The squeezing parameter r and frequency ω_β are plotted in Fig. 3, and the anisotropy strength is set as $\lambda = 5$ GHz. It is shown that the large squeezing at GHz frequencies can be achieved, e.g., $r \approx 2.6$, $\omega_\beta \approx 1.5$ GHz at $\omega_m/2\lambda = 1.01$, and $r \approx 2$, $\omega_\beta \approx 2.7$ GHz at $\omega_m/2\lambda = 1.04$. Operating at GHz frequencies, squeezed magnons are compatible with the microwave cavity as well as the optical Fabry-Perot cavity with a tunable free spectral range [33].

Therefore, the essential requirement is a strong anisotropy field. For YIG thin film, an effective anisotropy field H_u on the order of several hundred Oe has been demonstrated [78–80], which corresponds to an anisotropy energy in the GHz range. As estimated in the reference [70], $H_u \approx 800$ Oe corresponds to an anisotropy coefficient $\lambda \approx 2.8$ GHz. Furthermore, by utilizing high lattice-mismatch substrates to introduce substantial epitaxial strain, it demonstrates that a strong effective anisotropy field of 2800 Oe can be achieved in ultra-thin YIG while preserving low Gilbert damping [81]. The large anisotropy field ensures that obtaining high squeezing at GHz frequencies is theoretically sound and within the reach of modern nanofabrication and field-tuning capabilities.

4 Enhancement of the microwave-to-optics conversion efficiency

In this section, we study the enhancement of the microwave-to-optics conversion efficiency based on the enhanced coupling and cooperativity. For the effective Hamiltonian

H_{eff}, the Langevin equations of the coupled system can be written as

$$\frac{da_1}{dt} = -i\Delta_1 a_1 - i\tilde{G}_{\text{om}}\beta - \frac{\kappa_{\text{a}}}{2}a_1 + \sqrt{\kappa_{\text{a,ex}}}a_{1,\text{in}}, \tag{14a}$$

$$\frac{d\beta}{dt} = -i\omega_\beta \beta - i\tilde{G}_{\text{om}}a_1 - i\tilde{g}_{\text{em}}c - \frac{\gamma}{2}\beta, \tag{14b}$$

$$\frac{dc}{dt} = -i\omega_c c - i\tilde{g}_{\text{em}}\beta - \frac{\kappa_{\text{c}}}{2}c + \sqrt{\kappa_{\text{c,ex}}}c_{\text{in}}, \tag{14c}$$

where $\kappa_{\text{a,ex}}$ and $\kappa_{\text{c,ex}}$ are the external coupling rates, and $a_{1,\text{in}}$ and c_{in} denote the input field for optical and microwave modes, respectively. In the study of magnon-mediated microwave-optical conversion, the high amplitude of the input field results in a large signal-to-noise ratio, making the noise contribution insignificant for the conversion efficiency, and we have neglected the noise terms for simplicity.

In the frequency domain, the Langevin equations can be solved using the Fourier transform

$$a_1 = \chi_a(-i\tilde{G}_{\text{om}}\beta + \sqrt{\kappa_{\text{a,ex}}}a_{1,\text{in}}), \tag{15a}$$

$$\beta = \chi_\beta(-i\tilde{G}_{\text{om}}a_1 - i\tilde{g}_{\text{em}}c), \tag{15b}$$

$$c = \chi_c(-i\tilde{g}_{\text{em}}\beta + \sqrt{\kappa_{\text{c,ex}}}c_{\text{in}}), \tag{15c}$$

where the susceptibilities are given as $\chi_a = [-i(\omega - \Delta_1) + \kappa_{\text{a}}/2]^{-1}$, $\chi_\beta = [-i(\omega - \omega_\beta) + \gamma/2]^{-1}$ and $\chi_c = [-i(\omega - \omega_c) + \kappa_{\text{c}}/2]^{-1}$. For the microwave-to-optics conversion process, we consider that the input signal comes from a microwave field and set the optical input $a_{1,\text{in}} = 0$. Using the input-output relation $a_{1,\text{out}} = a_{1,\text{in}} - \sqrt{\kappa_{\text{a,ex}}}a_1$ [82], the conversion efficiency is given by

$$\tilde{\eta} = \frac{\langle a_{1,\text{out}}^\dagger a_{1,\text{out}}\rangle}{\langle c_{\text{in}}^\dagger c_{\text{in}}\rangle} = \left|\frac{\tilde{G}_{\text{om}}\tilde{g}_{\text{em}}\sqrt{\kappa_{\text{a,ex}}}\sqrt{\kappa_{\text{c,ex}}}}{\chi_a^{-1}\chi_\beta^{-1}\chi_c^{-1} + \chi_c^{-1}\tilde{G}_{\text{om}}^2 + \chi_a^{-1}\tilde{g}_{\text{em}}^2}\right|^2. \tag{16}$$

The spectra of the conversion efficiency $\tilde{\eta}$ is plotted in Fig. 4(a). The maximum conversion efficiency is achieved under the triple-resonance condition $\omega = \omega_\beta = \Delta_1 = \omega_c$. In conventional magnon-mediated microwave-to-optical frequency conversion, the condition $\omega_m = \Delta_1$ is required to maximize the Brillouin light scattering [45]. Here, however, the scattering process is mediated by the squeezed magnon mode, and its efficiency is maximized when $\omega_\beta = \Delta_1 = \omega_1 - \omega_2$. When the frequency ω_β deviates from the detuning Δ_1, the scattering efficiency will decrease rapidly, which in turn causes a sharp drop in the microwave-to-optical conversion efficiency. Figure 4(b) shows the conversion efficiency for different squeezings, the frequency of the squeezed mode is chosen as $\omega_\beta = \Delta_1$. Compared with the unsqueezing case $r = 0$, the conversion efficiency $\tilde{\eta}$ can be enhanced by several orders of magnitude when $r = 3$.

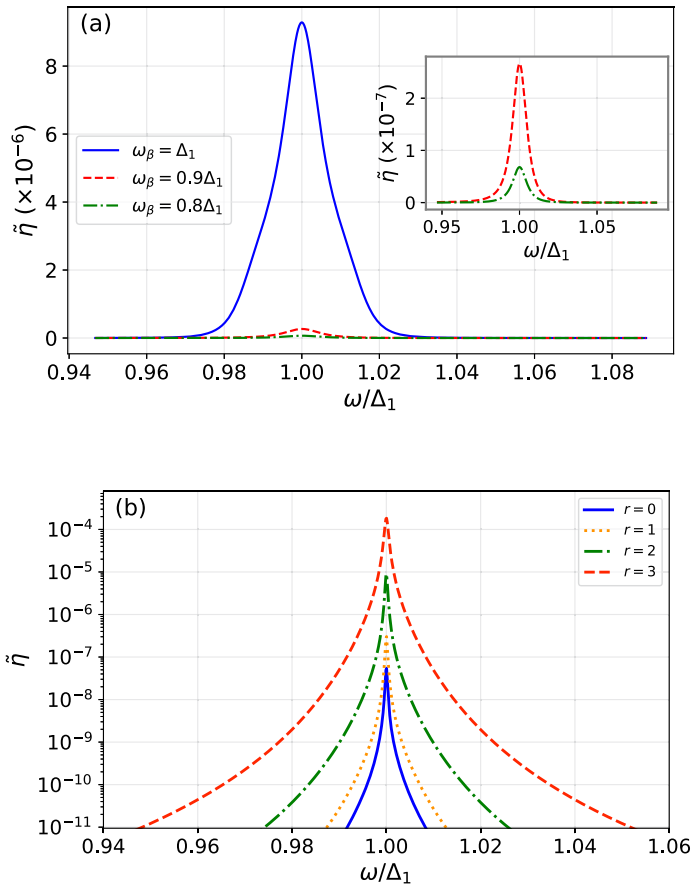

Figure 4 (Color online) (a) The conversion efficiency $\tilde{\eta}$ versus ω/Δ_1. The inset is an enlarged version of $\omega_\beta/\Delta_1 = 0.9$ and $\omega_\beta/\Delta_1 = 0.8$ in the figure. The squeezing parameter is set as $r = 3$. The parameters adopted from Ref. [32] are: $\Delta_1/2\pi = \omega_c/2\pi = 8.45$ GHz, $G_{\rm om}/2\pi = 22.59$ kHz, $g_{\rm em}/2\pi = 13.3$ MHz, $\kappa_{\rm c}/2\pi = 250$ MHz, $\kappa_{\rm c,ex}/2\pi = 165$ MHz, $\gamma/2\pi = 3.6$ MHz. The dissipation rates of the optical mode are chosen as $\kappa_{\rm a}/2\pi = 100$ MHz and $\kappa_{\rm a,ex}/2\pi = 50$ MHz. (b) The conversion efficiency $\tilde{\eta}$ versus ω/Δ_1 for different squeezing, the frequency of squeezed mode is set $\omega_\beta = \Delta_1$, and the magnetic-dipole coupling is $g_{\rm em}/2\pi = 1.33$ MHz

Under the triple-resonance condition, the conversion efficiency simplifies to $\tilde{\eta} = \eta_o\eta_e\tilde{\eta}_{\rm in}$ with the extraction factors $\eta_o = \kappa_{\rm a,ex}/\kappa_{\rm a}$ and $\eta_e = \kappa_{\rm c,ex}/\kappa_{\rm c}$, and the internal conversion efficiency

$$\tilde{\eta}_{\rm in} = \frac{4\tilde{C}_{\rm om}\tilde{C}_{\rm em}}{(1+\tilde{C}_{\rm om}+\tilde{C}_{\rm em})^2}. \tag{17}$$

The internal conversion efficiency approaches unity, $\tilde{\eta}_{\rm in} \to 1$, when both cooperativities satisfy $\tilde{C}_{\rm om} = \tilde{C}_{\rm em} \gg 1$. While a magneto-microwave cooperativity of $C_{\rm em} = 0.8$ has been experimentally demonstrated, the magneto-optical cooperativity remains very small ($C_{\rm om} \sim 10^{-7}$) [32], due to the weak single-photon magneto-optical coupling. With this value of $C_{\rm om}$, the enhanced magneto-optical cooperativity $\tilde{C}_{\rm om} = C_{\rm om}\cosh^2(r)$ is still small even for large squeezing parameter r. For $\tilde{C}_{\rm om} \ll 1$, we can obtain from Eq. (17) that the maximum value of $\tilde{\eta}_{\rm in}$ exist at $\tilde{C}_{\rm em} = 1$, not the large magneto-microwave cooperativity $\tilde{C}_{\rm em} \gg 1$. The internal conversion efficiency $\tilde{\eta}_{\rm in}$ versus the squeezing parameter r for dif-

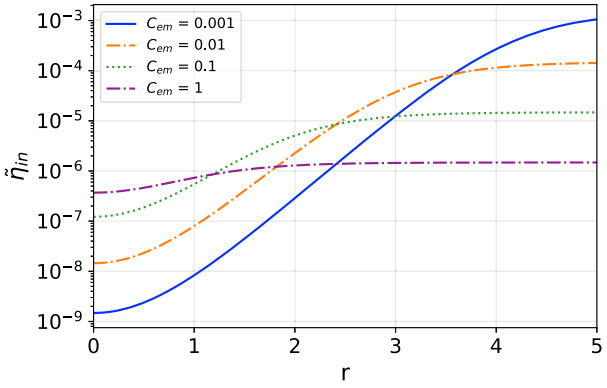

Figure 5 (Color online) The internal conversion efficiency $\tilde{\eta}_{\text{in}}$ as a function of squeezing for different values of C_{em}, the magneto-optical cooperativity is chosen as $C_{\text{om}} = 4 \times 10^{-7}$

ferent values of C_{em} is plotted in Fig. 5, where the magneto-optical cooperativity is chosen as $C_{\text{om}} = 4 \times 10^{-7}$. It is shown that for small C_{em} the $\tilde{\eta}_{\text{in}}$ increases rapidly as increasing squeezing r, but the conversion efficiency is only slightly enhanced by squeezing for large magneto-microwave cooperativity ($C_{\text{em}} = 1$ and hence $\tilde{C}_{\text{em}} = C_{\text{em}} \cosh^2(r) \gg 1$). By properly choosing the magneto-microwave coupling g_{em} and the cooperativity C_{em}, the internal conversion efficiency can be increased by several orders of magnitude by the squeezing, e.g., for $C_{\text{em}} = 0.01$, the internal conversion efficiency $\tilde{\eta}_{\text{in}} \sim 10^{-8}$ is enhanced to $\tilde{\eta}_{\text{in}} \sim 10^{-5}$ when squeezing parameter $r = 3$.

5 Conclusion

In conclusion, we have proposed a scheme to alleviate the fundamental limitation of weak optomagnonic coupling in magnon-mediated microwave-optical frequency conversion. By exploiting the intrinsic magnetic shape anisotropy of a YIG thin film, the magnon mode is naturally squeezed, leading to amplified quantum fluctuations. We demonstrated that this squeezed state enhances both the optomagnonic and magneto-microwave interactions, which in turn dramatically increases the cooperativity of the system and the overall conversion efficiency. Under the triple-resonance condition, the internal conversion efficiency can be improved by several orders of magnitude for a large magnon squeezing. Our scheme highlights the potential of magnon squeezing as an intrinsic resource that provides a stable and experimentally feasible approach for achieving high-efficiency microwave-optical frequency conversion.

Appendix: Derivation of the squeezing Hamiltonian

Using the spin raising and lowering operators, define that

$$S_x = (S^+ + S^-)/2, \tag{A.1a}$$

$$S_y = (S^+ - S^-)/2i, \tag{A.1b}$$

then the ferromagnetic Hamiltonian Eq. (2) can be expressed as

$$H_m = -2J\sum_{\langle i,j\rangle}[\frac{1}{2}(S_i^+S_j^- + S_i^-S_j^+) + S_{iz}S_{jz}] - g_Z\mu_B B_0\sum_i S_{iz} \tag{A.2}$$
$$+\sum_i[\frac{1}{4}(K_x-K_y)(S_i^{+2}+S_i^{-2}) + \frac{1}{4}(K_x+K_y)(S_i^+S_i^- + S_i^-S_i^+) + K_zS_{iz}^2].$$

Applying the Holstein-Primakoff transformation $S_i^+ \approx \sqrt{2S}m_i$, $S_i^- \approx \sqrt{2S}m_i^\dagger$, and $S_{iz} \approx S - m_i^\dagger m_i$, where S is the total spin. The ferromagnetic Hamiltonian becomes

$$H_m = -2JS\sum_{\langle i,j\rangle}(m_i^\dagger m_j + m_i m_j^\dagger - m_i^\dagger m_i - m_j^\dagger m_j) + g_Z\mu_B B_0\sum_i m_i^\dagger m_i \tag{A.3}$$
$$+\sum_i[\frac{S}{2}(K_x-K_y)(m_i^{\dagger 2}+m_i^2) + S(K_x+K_y-2K_z)m_i^\dagger m_i + K_z(m_i^\dagger m_i)^2],$$

where we have omitted constant terms and kept the terms in the exchange interaction up to second order in creation/annihilation operators. The general form of the magnetic anisotropy introduces both the quadratic term $\frac{S}{2}(K_x-K_y)(m_i^{\dagger 2}+m_i^2)$ and the Kerr nonlinearity $K_z(m_i^\dagger m_i)^2$. Here, we focus on the squeezing properties of magnons, which originate from the difference between in-plane anisotropies $(K_x - K_y)$. The Kerr nonlinearity, proportional to K_z, constitutes a higher-order perturbation in the low-excitation regime we consider. Its energy scale is significantly smaller than the dominant quadratic term, and thus it can be safely neglected in our linearized analysis. This treatment is consistent with the focus on the leading-order (quadratic) effects of anisotropy.

The bosonic operators defined on each site are related to the spin-wave operators via the Fourier transforms

$$m_i = N^{-1/2}\sum_{\mathbf{k}} m_{\mathbf{k}}e^{i\mathbf{k}\cdot\mathbf{r}_i}, \tag{A.4a}$$

$$m_i^\dagger = N^{-1/2}\sum_{\mathbf{k}} m_{\mathbf{k}}^\dagger e^{-i\mathbf{k}\cdot\mathbf{r}_i}. \tag{A.4b}$$

where $m_{\mathbf{k}}$ ($m_{\mathbf{k}}^\dagger$) represents the magnon annihilation (creation) operator with the wavevector $\mathbf{k}$, and N is the total number of spins in the ferromagnet. The transformation of the first two terms in Eq. (A.3) has been discussed in detail in Ref. [34]. In the long wavelength limit, the first two terms can be transformed as

$$-2JS\sum_{\langle i,j\rangle}(m_i^\dagger m_j + m_i m_j^\dagger - m_i^\dagger m_i - m_j^\dagger m_j) + g_Z\mu_B B_0\sum_i m_i^\dagger m_i \tag{A.5}$$
$$=(4JS\mathrm{k}^2a^2 + g_Z\mu_B B_0)m_{\mathbf{k}}^\dagger m_{\mathbf{k}},$$

where $\mathrm{k} = |\mathbf{k}|$ is the momentum and a is the lattice parameter. Here, we focus on the transformation of the anisotropic Hamiltonian. Using the Fourier transforms, the quadratic

term becomes

$$\sum_i \frac{S}{2}(K_x - K_y)(m_i^{\dagger 2} + m_i^2) \tag{A.6}$$
$$= \frac{S}{2}(K_x - K_y) \sum_{i\mathbf{k}\mathbf{k}'} \frac{1}{N}[e^{-\mathrm{i}(\mathbf{k}+\mathbf{k}')\cdot\mathbf{r}_i} m_{\mathbf{k}}^\dagger m_{\mathbf{k}'}^\dagger + e^{\mathrm{i}(\mathbf{k}+\mathbf{k}')\cdot\mathbf{r}_i} m_{\mathbf{k}} m_{\mathbf{k}'}].$$

Due to the periodicity of the crystal, one has $\frac{1}{N}\sum_i e^{-\mathrm{i}(\mathbf{k}+\mathbf{k}')\cdot\mathbf{r}_i} = \delta_{\mathbf{k},-\mathbf{k}'}$. Then, we have

$$\sum_i \frac{S}{2}(K_x - K_y)(m_i^{\dagger 2} + m_i^2) = \frac{S}{2}(K_x - K_y) \sum_{\mathbf{k}} (m_{\mathbf{k}}^\dagger m_{-\mathbf{k}}^\dagger + m_{\mathbf{k}} m_{-\mathbf{k}}). \tag{A.7}$$

Through similar calculations, the second term in the anisotropic Hamiltonian is

$$S(K_x + K_y - 2K_z) \sum_i m_i^\dagger m_i = S(K_x + K_y - 2K_z) \sum_{\mathbf{k}} m_{\mathbf{k}}^\dagger m_{\mathbf{k}}. \tag{A.8}$$

Therefore, we obtain the transformed ferromagnetic Hamiltonian

$$H_m = [4JS\mathrm{k}^2 a^2 + g_Z \mu_B B_0 + S(K_x + K_y - 2K_z)] m_{\mathbf{k}}^\dagger m_{\mathbf{k}} \tag{A.9}$$
$$+ \frac{S}{2}(K_x - K_y) \sum_{\mathbf{k}} (m_{\mathbf{k}}^\dagger m_{-\mathbf{k}}^\dagger + m_{\mathbf{k}} m_{-\mathbf{k}}),$$

which is the Hamiltonian Eq. (3) in the main tex.

Author contributions
Hong Xie conceived the research concept and wrote the original draft. Le-Wei He and Xiang Lin performed the formal analysis and modification of the manuscript. Xiu-Min Lin supervised the entire research process. All authors reviewed the manuscript.

Funding information
This work was supported by the National Natural Science Foundation of China (Grants No. 12174054 and No. 12274079), the Natural Science Foundation of Fujian Province of China (Grants No. 2025J011104 and No. 2022J02027).

Data availability
No datasets were generated or analysed during the current study.

Declarations

Competing interests
The authors declare no competing interests.

Author details
[1]Department of Mathematics and Physics, Fujian Jiangxia University, Fuzhou, 350108, China. [2]Fujian Provincial Key Laboratory of Quantum Manipulation and New Energy Materials, College of Physics and Energy, Fujian Normal University, Fuzhou, 350117, China. [3]Fujian Provincial Engineering Technology Research Center of Solar Energy Conversion and Energy Storage, Fuzhou, 350117, China. [4]Fujian Provincial Collaborative Innovation Center for Advanced High-Field Superconducting Materials and Engineering, Fuzhou, 350117, China.

Received: 9 November 2025 Accepted: 18 December 2025 Published online: 30 December 2025

References

1. Lambert NJ, Rueda A, Sedlmeir F, Schwefel HGL. Coherent conversion between microwave and optical photons—an overview of physical implementations. Adv Quantum Technol. 2020;3(1):1900077. https://doi.org/10.1002/qute.201900077.
2. Han X, Fu W, Zou C-L, Jiang L, Tang HX. Microwave-optical quantum frequency conversion. Optica. 2021;8(8):1050–64. https://doi.org/10.1364/OPTICA.425414.

3. Lauk N, Sinclair N, Barzanjeh S, Covey JP, Saffman M, Spiropulu M, Simon C. Perspectives on quantum transduction. Quantum Sci Technol. 2020;5(2):020501. https://doi.org/10.1088/2058-9565/ab788a.
4. Mirhosseini M, Sipahigil A, Kalaee M, Painter O. Superconducting qubit to optical photon transduction. Nature. 2020;588(7839):599–603.
5. Andrews RW, Peterson RW, Purdy TP, Cicak K, Simmonds RW, Regal CA, Lehnert KW. Bidirectional and efficient conversion between microwave and optical light. Nat Phys. 2014;10(4):321–6.
6. Arnold G, Wulf M, Barzanjeh S, Redchenko E, Rueda A, Hease WJ, Hassani F, Fink JM. Converting microwave and telecom photons with a silicon photonic nanomechanical interface. Nat Commun. 2020;11(1):4460.
7. Peairs G, Chou M-H, Bienfait A, Chang H-S, Conner C, Dumur É, Grebel J, Povey R, Şahin E, Satzinger K, et al. Continuous and time-domain coherent signal conversion between optical and microwave frequencies. Phys Rev Appl. 2020;14(6):061001.
8. Delaney R, Urmey M, Mittal S, Brubaker B, Kindem J, Burns P, Regal C, Lehnert K. Superconducting-qubit readout via low-backaction electro-optic transduction. Nature. 2022;606(7914):489–93.
9. Bochmann J, Vainsencher A, Awschalom DD, Cleland AN. Nanomechanical coupling between microwave and optical photons. Nat Phys. 2013;9(11):712–6.
10. Forsch M, Stockill R, Wallucks A, Marinković I, Gärtner C, Norte RA, Otten F, Fiore A, Srinivasan K, Gröblacher S. Microwave-to-optics conversion using a mechanical oscillator in its quantum ground state. Nat Phys. 2020;16(1):69–74.
11. Jiang W, Sarabalis CJ, Dahmani YD, Patel RN, Mayor FM, McKenna TP, Van Laer R, Safavi-Naeini AH. Efficient bidirectional piezo-optomechanical transduction between microwave and optical frequency. Nat Commun. 2020;11(1):1166.
12. Hönl S, Popoff Y, Caimi D, Beccari A, Kippenberg TJ, Seidler P. Microwave-to-optical conversion with a gallium phosphide photonic crystal cavity. Nat Commun. 2022;13(1):2065.
13. Stockill R, Forsch M, Hijazi F, Beaudoin G, Pantzas K, Sagnes I, Braive R, Gröblacher S. Ultra-low-noise microwave to optics conversion in gallium phosphide. Nat Commun. 2022;13(1):6583.
14. Rueda A, Sedlmeir F, Collodo MC, Vogl U, Stiller B, Schunk G, Strekalov DV, Marquardt C, Fink JM, Painter O, et al. Efficient microwave to optical photon conversion: an electro-optical realization. Optica. 2016;3(6):597–604.
15. Witmer JD, McKenna TP, Arrangoiz-Arriola P, Van Laer R, Wollack EA, Lin F, Jen AK, Luo J, Safavi-Naeini AH. A silicon-organic hybrid platform for quantum microwave-to-optical transduction. Quantum Sci Technol. 2020;5(3):034004.
16. McKenna TP, Witmer JD, Patel RN, Jiang W, Van Laer R, Arrangoiz-Arriola P, Wollack EA, Herrmann JF, Safavi-Naeini AH. Cryogenic microwave-to-optical conversion using a triply resonant lithium-niobate-on-sapphire transducer. Optica. 2020;7(12):1737–45.
17. Xu Y, Sayem AA, Fan L, Zou C-L, Wang S, Cheng R, Fu W, Yang L, Xu M, Tang HX. Bidirectional interconversion of microwave and light with thin-film lithium niobate. Nat Commun. 2021;12(1):4453.
18. Sahu R, Hease W, Rueda A, Arnold G, Qiu L, Fink JM. Quantum-enabled operation of a microwave-optical interface. Nat Commun. 2022;13(1):1276.
19. Wang C, Gonin I, Grassellino A, Kazakov S, Romanenko A, Yakovlev VP, Zorzetti S. High-efficiency microwave-optical quantum transduction based on a cavity electro-optic superconducting system with long coherence time. npj Quantum Inf. 2022;8(1):149.
20. Han J, Vogt T, Gross C, Jaksch D, Kiffner M, Li W. Coherent microwave-to-optical conversion via six-wave mixing in Rydberg atoms. Phys Rev Lett. 2018;120(9):093201.
21. Vogt T, Gross C, Han J, Pal SB, Lam M, Kiffner M, Li W. Efficient microwave-to-optical conversion using Rydberg atoms. Phys Rev A. 2019;99(2):023832.
22. Tu H-T, Liao K-Y, Zhang Z-X, Liu X-H, Zheng S-Y, Yang S-Z, Zhang X-D, Yan H, Zhu S-L. High-efficiency coherent microwave-to-optics conversion via off-resonant scattering. Nat Photonics. 2022;16(4):291–6.
23. Gallagher LA, Rogers JP, Pritchett JD, Mistry RA, Pizzey D, Adams CS, Jones MP, Grünwald P, Walther V, Hodges C, et al. Microwave-optical coupling via Rydberg excitons in cuprous oxide. Phys Rev Res. 2022;4(1):013031.
24. Kumar A, Suleymanzade A, Stone M, Taneja L, Anferov A, Schuster DI, Simon J. Quantum-enabled millimetre wave to optical transduction using neutral atoms. Nature. 2023;615(7953):614–9.
25. Borówka S, Pylypenko U, Mazelanik M, Parniak M. Continuous wideband microwave-to-optical converter based on room-temperature Rydberg atoms. Nat Photonics. 2024;18(1):32–8.
26. Rochman J, Xie T, Bartholomew JG, Schwab K, Faraon A. Microwave-to-optical transduction with erbium ions coupled to planar photonic and superconducting resonators. Nat Commun. 2023;14(1):1153.
27. Hisatomi R, Osada A, Tabuchi Y, Ishikawa T, Noguchi A, Yamazaki R, Usami K, Nakamura Y. Bidirectional conversion between microwave and light via ferromagnetic magnons. Phys Rev B. 2016;93(17):174427.
28. Zhang X, Zhu N, Zou C-L, Tang HX. Optomagnonic whispering gallery microresonators. Phys Rev Lett. 2016;117(12):123605.
29. Osada A, Hisatomi R, Noguchi A, Tabuchi Y, Yamazaki R, Usami K, Sadgrove M, Yalla R, Nomura M, Nakamura Y. Cavity optomagnonics with spin-orbit coupled photons. Phys Rev Lett. 2016;116:223601. https://doi.org/10.1103/PhysRevLett.116.223601.
30. Haigh J, Nunnenkamp A, Ramsay A, Ferguson A. Triple-resonant Brillouin light scattering in magneto-optical cavities. Phys Rev Lett. 2016;117(13):133602.
31. Bartholomew JG, Rochman J, Xie T, Kindem JM, Ruskuc A, Craiciu I, Lei M, Faraon A. On-chip coherent microwave-to-optical transduction mediated by ytterbium in yvo4. Nat Commun. 2020;11(1):3266.
32. Zhu N, Zhang X, Han X, Zou C-L, Zhong C, Wang C-H, Jiang L, Tang HX. Waveguide cavity optomagnonics for microwave-to-optics conversion. Optica. 2020;7(10):1291–7. https://doi.org/10.1364/OPTICA.397967.
33. Wu W-J, Wang Y-P, Li J, Li G, You J-Q. Microwave-to-optics conversion using magnetostatic modes and a tunable optical cavity. Laser Photonics Rev. 2025;19(2):2400648. https://doi.org/10.1002/lpor.202400648.
34. Stancil DD, Prabhakar A. Spin waves: theory and applications. New York: Springer; 2009.
35. Soykal OO, Flatté ME. Strong field interactions between a nanomagnet and a photonic cavity. Phys Rev Lett. 2010;104:077202. https://doi.org/10.1103/PhysRevLett.104.077202.

36. Huebl H, Zollitsch CW, Lotze J, Hocke F, Greifenstein M, Marx A, Gross R, Goennenwein STB. High cooperativity in coupled microwave resonator ferrimagnetic insulator hybrids. Phys Rev Lett. 2013;111:127003. https://doi.org/10.1103/PhysRevLett.111.127003.
37. Tabuchi Y, Ishino S, Ishikawa T, Yamazaki R, Usami K, Nakamura Y. Hybridizing ferromagnetic magnons and microwave photons in the quantum limit. Phys Rev Lett. 2014;113:083603. https://doi.org/10.1103/PhysRevLett.113.083603.
38. Zhang X, Zou C-L, Jiang L, Tang HX. Strongly coupled magnons and cavity microwave photons. Phys Rev Lett. 2014;113:156401. https://doi.org/10.1103/PhysRevLett.113.156401.
39. Zhang X, Zou C-L, Jiang L, Tang HX. Cavity magnomechanics. Sci Adv. 2016;2(3):1501286. https://doi.org/10.1126/sciadv.1501286.
40. Tabuchi Y, Ishino S, Noguchi A, Ishikawa T, Yamazaki R, Usami K, Nakamura Y. Coherent coupling between a ferromagnetic magnon and a superconducting qubit. Science. 2015;349(6246):405–8.
41. Lachance-Quirion D, Tabuchi Y, Ishino S, Noguchi A, Ishikawa T, Yamazaki R, Nakamura Y. Resolving quanta of collective spin excitations in a millimeter-sized ferromagnet. Sci Adv. 2017;3(7):1603150.
42. Xu D, Gu X-K, Li H-K, Weng Y-C, Wang Y-P, Li J, Wang H, Zhu S-Y, You J. Quantum control of a single magnon in a macroscopic spin system. Phys Rev Lett. 2023;130(19):193603.
43. Lachance-Quirion D, Tabuchi Y, Gloppe A, Usami K, Nakamura Y. Hybrid quantum systems based on magnonics. Appl Phys Express. 2019;12(7):070101.
44. Yuan HY, Cao Y, Kamra A, Duine RA, Yan P. Quantum magnonics: when magnon spintronics meets quantum information science. Phys Rep. 2022;965:1–74. https://doi.org/10.1016/j.physrep.2022.03.002.
45. Zare Rameshti B, Viola Kusminskiy S, Haigh JA, Usami K, Lachance-Quirion D, Nakamura Y, Hu C-M, Tang HX, Bauer GEW, Blanter YM. Cavity magnonics. Phys Rep. 2022;979:1–61. https://doi.org/10.1016/j.physrep.2022.06.001.
46. Kostylev N, Goryachev M, Tobar ME. Superstrong coupling of a microwave cavity to yttrium iron garnet magnons. Appl Phys Lett. 2016;108(6):062402. https://doi.org/10.1063/1.4941730.
47. Graf J, Pfeifer H, Marquardt F, Viola Kusminskiy S. Cavity optomagnonics with magnetic textures: coupling a magnetic vortex to light. Phys Rev B. 2018;98:241406. https://doi.org/10.1103/PhysRevB.98.241406.
48. Sharma S, Rameshti BZ, Blanter YM, Bauer GEW. Optimal mode matching in cavity optomagnonics. Phys Rev B. 2019;99:214423. https://doi.org/10.1103/PhysRevB.99.214423.
49. Haigh JA, Chakalov RA, Ramsay AJ. Subpicoliter magnetoptical cavities. Phys Rev Appl. 2020;14:044005. https://doi.org/10.1103/PhysRevApplied.14.044005.
50. Bittencourt VASV, Liberal I, Viola Kusminskiy S. Optomagnonics in dispersive media: magnon-photon coupling enhancement at the epsilon-near-zero frequency. Phys Rev Lett. 2022;128:183603. https://doi.org/10.1103/PhysRevLett.128.183603.
51. Haigh JA, Nunnenkamp A, Ramsay AJ. Polarization dependent scattering in cavity optomagnonics. Phys Rev Lett. 2021;127:143601. https://doi.org/10.1103/PhysRevLett.127.143601.
52. Engelhardt F, Bittencourt VA, Huebl H, Klein O, Kusminskiy SV. Optimal broadband frequency conversion via a magnetomechanical transducer. Phys Rev Appl. 2022;18(4):044059.
53. Lü XY, Wu Y, Johansson JR, Jing H, Zhang J, Nori F. Squeezed optomechanics with phase-matched amplification and dissipation. Phys Rev Lett. 2015;114(9):093602.
54. Lemonde M-A, Didier N, Clerk AA. Enhanced nonlinear interactions in quantum optomechanics via mechanical amplification. Nat Commun. 2016;7(1):11338.
55. Qin W, Miranowicz A, Li P-B, Lü X-Y, You J-Q, Nori F. Exponentially enhanced light-matter interaction, cooperativities, and steady-state entanglement using parametric amplification. Phys Rev Lett. 2018;120(9):093601.
56. Leroux C, Govia LCG, Clerk AA. Enhancing cavity quantum electrodynamics via antisqueezing: synthetic ultrastrong coupling. Phys Rev Lett. 2018;120(9):093602.
57. Ge W, Sawyer BC, Britton JW, Jacobs K, Bollinger JJ, Foss-Feig M. Trapped ion quantum information processing with squeezed phonons. Phys Rev Lett. 2019;122(3):030501.
58. Wang Y, Li C, Sampuli EM, Song J, Jiang Y, Xia Y. Enhancement of coherent dipole coupling between two atoms via squeezing a cavity mode. Phys Rev A. 2019;99(2):023833.
59. Li P-B, Zhou Y, Gao W-B, Nori F. Enhancing spin-phonon and spin-spin interactions using linear resources in a hybrid quantum system. Phys Rev Lett. 2020;125(15):153602.
60. Chen Y-H, Qin W, Wang X, Miranowicz A, Nori F. Shortcuts to adiabaticity for the quantum Rabi model: efficient generation of giant entangled cat states via parametric amplification. Phys Rev Lett. 2021;126(2):023602.
61. Burd SC, Srinivas R, Knaack HM, Ge W, Wilson AC, Wineland DJ, Leibfried D, Bollinger JJ, Allcock D, Slichter D. Quantum amplification of boson-mediated interactions. Nat Phys. 2021;17(8):898–902.
62. Xie H, He L-W, Shang X, Lin X-M. Phonon blockade in a squeezed cavity optomechanical system. Adv Quantum Technol. 2024;7(1):2300239. https://doi.org/10.1002/qute.202300239.
63. Xie H, He L-W, Shang X, Lin X-M. Photon blockade in cavity optomechanics via parametric amplification. Adv Quantum Technol. 2024;7(9):2400065.
64. Kamra A, Belzig W. Super-Poissonian shot noise of squeezed-magnon mediated spin transport. Phys Rev Lett. 2016;116:146601. https://doi.org/10.1103/PhysRevLett.116.146601.
65. Kamra A, Belzig W, Brataas A. Magnon-squeezing as a niche of quantum magnonics. Appl Phys Lett. 2020;117(9).
66. Zou J, Kim SK, Tserkovnyak Y. Tuning entanglement by squeezing magnons in anisotropic magnets. Phys Rev B. 2020;101:014416. https://doi.org/10.1103/PhysRevB.101.014416.
67. Sharma S, Bittencourt VASV, Karenowska AD, Kusminskiy SV. Spin cat states in ferromagnetic insulators. Phys Rev B. 2021;103:100403. https://doi.org/10.1103/PhysRevB.103.L100403.
68. Holstein T, Primakoff H. Field dependence of the intrinsic domain magnetization of a ferromagnet. Phys Rev. 1940;58:1098–113. https://doi.org/10.1103/PhysRev.58.1098.
69. Yuan HY, Duine RA. Magnon antibunching in a nanomagnet. Phys Rev B. 2020;102:100402. https://doi.org/10.1103/PhysRevB.102.100402.
70. Lee JM, Lee H-W, Hwang M-J. Cavity magnonics with easy-axis ferromagnets: critically enhanced magnon squeezing and light-matter interaction. Phys Rev B. 2023;108:241404. https://doi.org/10.1103/PhysRevB.108.L241404.
71. Skogvoll IC, Lidal J, Danon J, Kamra A. Tunable anisotropic quantum Rabi model via a magnon–spin-qubit ensemble. Phys Rev Appl. 2021;16:064008. https://doi.org/10.1103/PhysRevApplied.16.064008.

72. Xie H, He L-W, Lin X, Shi Z-G, Lin X-M. Unconventional magnon blockade in an anisotropic ferromagnetic system. Phys Rev B. 2025;112:024406. https://doi.org/10.1103/77sf-w3k4.
73. Kusminskiy SV. Cavity optomagnonics. In: Optomagnonic structures: novel architectures for simultaneous control of light and spin waves. Singapore: World Scientific; 2021. p. 299–353.
74. Aspelmeyer M, Kippenberg TJ, Marquardt F. Cavity optomechanics. Rev Mod Phys. 2014;86(4):1391.
75. Liu Z-X, Wang B, Xiong H, Wu Y. Magnon-induced high-order sideband generation. Opt Lett. 2018;43(15):3698–701. https://doi.org/10.1364/OL.43.003698.
76. Liu Z-X, You C, Wang B, Xiong H, Wu Y. Phase-mediated magnon chaos-order transition in cavity optomagnonics. Opt Lett. 2019;44(3):507–10. https://doi.org/10.1364/OL.44.000507.
77. Liu Z-X, Li Y-Q. Optomagnonic frequency combs. Photon Res. 2022;10(12):2786–93. https://doi.org/10.1364/PRJ.467595.
78. Manuilov SA, Khartsev S, Grishin AM. Pulsed laser deposited y3fe5o12 films: nature of magnetic anisotropy I. J Appl Phys. 2009;106(12).
79. Wang H, Du C, Hammel PC, Yang F. Strain-tunable magnetocrystalline anisotropy in epitaxial $Y_3\mathbf{fe}_5\mathbf{o}_{12}$ thin films. Phys Rev B. 2014;89:134404. https://doi.org/10.1103/PhysRevB.89.134404.
80. Bhoi B, Kim B, Kim Y, Kim M-K, Lee J-H, Kim S-K. Stress-induced magnetic properties of pld-grown high-quality ultrathin yig films. J Appl Phys. 2018;123(20).
81. Ding J, Liu C, Zhang Y, Erugu U, Quan Z, Yu R, McCollum E, Mo S, Yang S, Ding H, Xu X, Tang J, Yang X, Wu M. Nanometer-thick yttrium iron garnet films with perpendicular anisotropy and low damping. Phys Rev Appl. 2020;14:014017. https://doi.org/10.1103/PhysRevApplied.14.014017.
82. Walls D, Milburn GJ. Quantum optics. Berlin: Springer; 2008.

Publisher's note